PHYSICAL REVIEW A **95**, 011601(R) (2017)

Exact out-of-time-ordered correlation functions for an interacting lattice fermion model

Naoto Tsuji,[1] Philipp Werner,[2] and Masahito Ueda[1,3]
[1]*RIKEN Center for Emergent Matter Science (CEMS), Wako 351-0198, Japan*
[2]*Department of Physics, University of Fribourg, 1700 Fribourg, Switzerland*
[3]*Department of Physics, University of Tokyo, Hongo, Tokyo 113-0033, Japan*
(Received 19 October 2016; published 3 January 2017)

Exact solutions for local equilibrium and nonequilibrium out-of-time-ordered correlation (OTOC) functions are obtained for a lattice fermion model with on-site interactions, namely, the Falicov-Kimball (FK) model, in the large dimensional and thermodynamic limit. Our approach is based on the nonequilibrium dynamical mean-field theory generalized to an extended Kadanoff-Baym contour. We find that the density-density OTOC is most enhanced at intermediate coupling around the metal-insulator phase transition. In the high-temperature limit, the OTOC remains nontrivially finite and interaction dependent, even though dynamical charge correlations probed by an ordinary response function are completely suppressed. We propose an experiment to measure OTOCs of fermionic lattice systems including the FK and Hubbard models in ultracold atomic systems.

DOI: 10.1103/PhysRevA.95.011601

There is a growing interest in the scrambling and spreading of information in quantum many-body systems in wide areas of physics ranging from condensed matter to black holes [1–22]. A useful measure to diagnose the sensitivity of time-evolving quantities on the initial condition is the out-of-time-ordered correlation (OTOC) function [23] of two operators W and V,

$$C(t) = -\langle [W(t), V(0)]^2 \rangle. \tag{1}$$

In the semiclassical picture, if we choose $W = p_j, V = p_k$, $C(t) \sim \langle [\partial p_j(t)/\partial q_k(0)]^2 \rangle$ (p_j and q_k are canonical momenta and coordinates), so that OTOCs reflect how the system is scrambled and the initial-condition dependence is amplified. In chaotic systems, OTOCs are expected to grow exponentially in time (butterfly effect). It has been conjectured based on the holographic principle that there is a universal bound for the exponential growth rate of OTOCs (analogous to the Lyapunov exponent) [9]. Recently, the OTOC has been analytically evaluated for the Sachdev-Ye-Kitaev (SYK) model, a model of fermions having all-to-all four-body random interactions without hopping [6,24–28]. It was found to show exactly such a chaotic behavior with the bound saturated [6].

An immediate question is how OTOCs grow in the lattice fermion models with short-range interactions that are typically used to describe strongly correlated condensed-matter systems. To evaluate Eq. (1), one needs to compute quantities such as $\langle W(t)V(0)W(t)V(0)\rangle$, which are incompatible with the usual time-ordered sequence of operators on the Keldysh or Kadanoff-Baym contour $\mathcal{C}$ ($0 \to t \to 0 \to -i\beta$, β is the initial inverse temperature) [29–31]. This is in contrast to ordinary response functions. For example, a nonlinear optical susceptibility is given by a combination of current correlators such as $\langle [[[j(t), j(t')], j(t'')], j(t''')]\rangle$ with a causality constraint $t \geqslant t' \geqslant t'' \geqslant t'''$ [32], which can always be defined on $\mathcal{C}$. Due to the unconventional ordering, OTOCs have not been much studied for correlated lattice fermion models. Up to now, OTOC functions have been calculated mostly by exact diagonalization for spin [10,13–15,19] and boson [16] systems of small size.

In this Rapid Communication, we generalize the nonequilibrium dynamical mean-field theory (DMFT) [33,34] to an extended Kadanoff-Baym contour, which allows one to calculate OTOC functions for lattice fermion models in the infinite-dimensional and thermodynamic limit. We apply this technique to the Falicov-Kimball (FK) model [35,36], which admits an exact solution due to infinitely many conserved quantities. The FK model exhibits intriguing properties such as a metal-insulator transition, non-Fermi-liquid behavior [36], and Anderson localization in two dimensions [37]. Its nonequilibrium aspects have also been studied [33,38–43]. We show that OTOCs provide yet another insight into the physics of this model, that cannot be obtained from ordinary response functions. Finally, we propose an experimental scheme with ultracold atoms to measure OTOCs in a fermion model.

We begin by noting that an out-of-time-ordered function $\langle W(t)V(0)W(t)V(0)\rangle$ is rewritten as

$$\begin{aligned}
&\frac{\mathrm{Tr}[e^{-\beta H(0)}\,\mathcal{U}(0,t)W\,\mathcal{U}(t,0)V\,\mathcal{U}(0,t)W\,\mathcal{U}(t,0)V]}{\mathrm{Tr}[e^{-\beta H(0)}]} \\
&= \frac{\mathrm{Tr}[\mathcal{T}_{\tilde{\mathcal{C}}}\, e^{-i\int_{\tilde{\mathcal{C}}} dt\, H(t)} W_{t_+} V_{0_c} W_{t_-} V_{0_-}]}{\mathrm{Tr}[\mathcal{T}_{\tilde{\mathcal{C}}}\, e^{-i\int_{\tilde{\mathcal{C}}} dt\, H(t)}]} \\
&\equiv \left\langle \mathcal{T}_{\tilde{\mathcal{C}}}\, W_{t_+} V_{0_c} W_{t_-} V_{0_-} \right\rangle,
\end{aligned}$$

where $\mathcal{U}(t,t')$ is the unitary evolution operator, $\tilde{\mathcal{C}}$ is a doubly folded Kadanoff-Baym contour with time running as $0(\equiv 0_-) \to t(\equiv t_-) \to 0(\equiv 0_c) \to t(\equiv t_+) \to 0\,(\equiv 0_+) \to -i\beta$ [see Fig. 1(a)] [44], and $\mathcal{T}_{\tilde{\mathcal{C}}}$ is the time-ordering operator along $\tilde{\mathcal{C}}$. We can also unfold the contour $\tilde{\mathcal{C}}$ as shown in Fig. 1(b), where time runs as $0 \to 2t \to 0 \to -i\beta$. From t to $2t$, the time evolution is reversed, i.e., the system evolves with the Hamiltonian $-H(2t - \bar{t})$ ($t \leqslant \bar{t} \leqslant 2t$). These two types of contours are equivalent. It is straightforward to extend a field theory from $\mathcal{C}$ to $\tilde{\mathcal{C}}$. The nonequilibrium Green's function is defined on $\tilde{\mathcal{C}}$ as $G(t,t') = -i\langle \mathcal{T}_{\tilde{\mathcal{C}}}\, c(t)c^\dagger(t')\rangle$ [c ($c^\dagger$) is the fermion annihilation (creation) operator]. By replacing $\mathcal{C}$ with $\tilde{\mathcal{C}}$, the nonequilibrium DMFT is generalized as explicitly constructed below.

We consider the FK model with the Hamiltonian

$$H(t) = \sum_{ij} J_{ij} c_i^\dagger c_j + \sum_i \left(-\mu n_i^c + E_f n_i^f\right) + U(t) \sum_i n_i^f n_i^c, \tag{2}$$

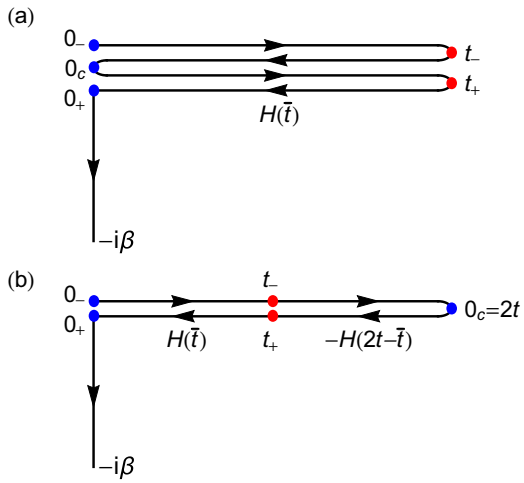

FIG. 1. Two types of extended [(a) doubly folded and (b) singly folded] Kadanoff-Baym contours $\tilde{\mathcal{C}}$, which are equivalent. In (a), the system evolves with the Hamiltonian $H(\bar{t})$ $(0 \leqslant \bar{t} \leqslant t)$, while in (b) the system evolves with $H(\bar{t})$ for $0 \leqslant \bar{t} \leqslant t$ and $-H(2t-\bar{t})$ for $t \leqslant \bar{t} \leqslant 2t$.

where $n_i^c \equiv c_i^\dagger c_i$, $n_i^f \equiv f_i^\dagger f_i$, J_{ij} and μ are the hopping amplitude and the chemical potential for the c particles, E_f is the energy level for the f particles, and $U(t)$ is the on-site interaction, which can be time dependent. The model is exactly solvable in any dimension in the sense that $[H,n_i^f]=0$ for all i, i.e., it has infinitely many conserved quantities. The immobile f particles act as a random potential for the itinerant c particles.

In the infinite-dimensional limit $(d \to \infty)$ with the hopping scaled as $J_{ij} \propto J_*/\sqrt{d}$ (J_* is a fixed constant) [45], the lattice model can be exactly mapped onto an impurity problem with a self-consistently determined dynamical mean field (hybridization function) $\Delta(t,t')$ [36,46–49], where the action is given by

$$\mathcal{S}_{\rm imp} = \int_{\tilde{\mathcal{C}}} dt dt'\, c^\dagger(t)\Delta(t,t')c(t') + \int_{\tilde{\mathcal{C}}} dt[-\mu n^c(t) + E_f n^f(t) + U(t)n^f(t)n^c(t)]. \quad (3)$$

The mapping is constructed such that the local lattice Green's function is equal to the impurity Green's function. In the large-d limit, the lattice self-energy becomes local and can be identified with the impurity self-energy. The single-particle Green's function for the FK model can be expressed as

$$G(t,t') \equiv -i\langle \mathcal{T}_{\tilde{\mathcal{C}}}\, c(t)c^\dagger(t')\rangle_{\mathcal{S}_{\rm imp}} = \sum_\alpha w_\alpha R_\alpha(t,t'), \quad (4)$$

where $\alpha = 0$ and 1 correspond to empty and occupied f-particle configurations, $w_1 = \langle n^f \rangle$, $w_0 = 1 - w_1$, and $R_\alpha(t,t')$ is a configuration-dependent Green's function, which satisfies the Dyson equation,

$$[i\partial_t + \mu - U(t)\alpha]R_\alpha(t,t') - \int_{\tilde{\mathcal{C}}} d\bar{t}\, \Delta(t,\bar{t})R_\alpha(\bar{t},t') = \delta_{\tilde{\mathcal{C}}}(t,t'). \quad (5)$$

Here, the integral is taken along the contour $\tilde{\mathcal{C}}$, and $\delta_{\tilde{\mathcal{C}}}(t,t')$ is the generalized contour delta function [50]. $R_0(t,t')$ is the usual Weiss Green's function in the nonequilibrium DMFT [34]. Throughout this Rapid Communication, we consider the half-filled case (i.e., $\mu = U/2$, $w_1 = 0.5$) on the Bethe lattice with infinite coordinations, with the density of states $D(\epsilon) = \sqrt{4J_*^2 - \epsilon^2}/(2\pi J_*^2)$, and use J_* (J_*^{-1}) as the unit of energy (time). In this case, $\Delta(t,t')$ is related to the local Green's function via $\Delta(t,t') = J_*^2 G(t,t')$ [49]. Within DMFT, the model shows a metal-to-Mott insulator transition at $U = 2$, and the metallic phase is a non-Fermi liquid [36].

In the FK model, the impurity action (3) can be block-diagonalized into f-particle configuration sectors ($\alpha = 0,1$), in which the c particles behave as free fermions in an effective potential $U(t)\alpha - \mu$. This makes it possible to calculate arbitrary local dynamical correlation functions exactly. Let us look at the two-point charge correlation function, which is given by the sum of contributions from the two sectors,

$$C_2(t_1,t_2) \equiv \langle \mathcal{T}_{\tilde{\mathcal{C}}}\, n^c(t_1)n^c(t_2)\rangle = \sum_\alpha w_\alpha \langle \mathcal{T}_{\tilde{\mathcal{C}}}\, n^c(t_1)n^c(t_2)\rangle_{\mathcal{S}_{\rm imp}^\alpha}, \quad (6)$$

where $\mathcal{S}_{\rm imp}^\alpha = \int_{\tilde{\mathcal{C}}} dt dt'\, c^\dagger(t)\Delta(t,t')c(t') + \int_{\tilde{\mathcal{C}}} dt[U(t)\alpha - \mu]c^\dagger(t)c(t)$ is the sector α $(n^f = \alpha)$ of the impurity action. Since $\mathcal{S}_{\rm imp}^\alpha$ is quadratic with respect to the c-particle operators, we can analytically evaluate the right-hand side of Eq. (6) by Wick's theorem [51]. The result is

$$C_2(t_1,t_2) = \sum_\alpha w_\alpha [R_\alpha(t_1,t_2)R_\alpha(t_2,t_1) - R_\alpha(t_1,t_1)R_\alpha(t_2,t_2)]. \quad (7)$$

Here, $R_\alpha(t,t')$ at equal times $(t = t')$ should be read as a lesser component (i.e., $t' = t + 0$). Equation (7) is symmetric with respect to the exchange $t_1 \leftrightarrow t_2$, and satisfies the boundary condition $\lim_{t_2 \to t_1} C_2(t_1,t_2) = \langle n^c(t_1)\rangle$.

As shown in Ref. [52], Eq. (7) correctly reproduces the previous result for the dynamical charge susceptibility [36,53–55]

$$\chi(t,t') = i\theta(t-t')\langle [n^c(t),n^c(t')]\rangle. \quad (8)$$

In the infinite-dimensional limit, the local dynamical charge susceptibility is equal to the lattice charge susceptibility $\chi_{\boldsymbol{q}}(t,t')$ at general momentum $\boldsymbol{q}$ (randomly chosen from the Brillouin zone), since $\chi(t,t') = N_{\boldsymbol{q}}^{-1}\sum_{\boldsymbol{q}} \chi_{\boldsymbol{q}}(t,t')$ and general momenta $\boldsymbol{q}$ make equal and dominant contributions to the momentum sum. In fact, we can confirm by explicit calculations that expression (7) gives the correct dynamical charge susceptibility for the general momentum [52].

The calculation can straightforwardly be generalized to arbitrary n-point local charge correlation functions. The three-point function is given by

$$\begin{aligned} &C_3(t_1,t_2,t_3) \\ &\equiv \langle \mathcal{T}_{\tilde{\mathcal{C}}}\, n^c(t_1)n^c(t_2)n^c(t_3)\rangle \\ &= \sum_\alpha w_\alpha \{ i[R_\alpha(t_1,t_2)R_\alpha(t_2,t_3)R_\alpha(t_3,t_1) + (1\text{ term})] \\ &\quad - i[R_\alpha(t_1,t_1)R_\alpha(t_2,t_3)R_\alpha(t_3,t_2) + (2\text{ terms})] \\ &\quad + iR_\alpha(t_1,t_1)R_\alpha(t_2,t_2)R_\alpha(t_3,t_3)\}, \end{aligned} \quad (9)$$

and the four-point function by

$$
\begin{aligned}
&C_4(t_1,t_2,t_3,t_4)\\
&\quad\equiv\langle\mathcal{T}_{\tilde{\mathcal{C}}}\, n^c(t_1)n^c(t_2)n^c(t_3)n^c(t_4)\rangle\\
&\quad=\sum_\alpha w_\alpha\{-[R_\alpha(t_1,t_2)R_\alpha(t_2,t_3)R_\alpha(t_3,t_4)R_\alpha(t_4,t_1)\\
&\qquad+(5\text{ terms})]\\
&\qquad+[R_\alpha(t_1,t_1)R_\alpha(t_2,t_3)R_\alpha(t_3,t_4)R_\alpha(t_4,t_2)+(7\text{ terms})]\\
&\qquad-[R_\alpha(t_1,t_1)R_\alpha(t_2,t_2)R_\alpha(t_3,t_4)R_\alpha(t_4,t_3)+(5\text{ terms})]\\
&\qquad+[R_\alpha(t_1,t_2)R_\alpha(t_2,t_1)R_\alpha(t_3,t_4)R_\alpha(t_4,t_3)+(2\text{ terms})]\\
&\qquad+R_\alpha(t_1,t_1)R_\alpha(t_2,t_2)R_\alpha(t_3,t_3)R_\alpha(t_4,t_4)\}. \qquad (10)
\end{aligned}
$$

In Eqs. (9) and (10), we group the terms by topologically equivalent Wick contractions, and in each group one representative term is spelled out. As a consistency check, one can see that the right-hand sides of Eqs. (9) and (10) are invariant under arbitrary permutations $t_i \leftrightarrow t_j$. We can also confirm that these correlation functions satisfy the boundary conditions $\lim_{t_3\to t_2} C_3(t_1,t_2,t_3) = C_2(t_1,t_2)$ and $\lim_{t_4\to t_3} C_4(t_1,t_2,t_3,t_4) = C_3(t_1,t_2,t_3)$.

The OTOC function (1) for $W = V = n^c$ can be expressed as

$$
\begin{aligned}
C(t) =& -C_4(t_+,0_c,t_-,0_-) - C_4(0_+,t_+,0_c,t_-)\\
&+C_3(t_+,0_c,t_-)+C_3(0_+,t_+,0_c), \qquad (11)
\end{aligned}
$$

where $t_\pm$, $0_\pm$, 0_c are the time points on $\tilde{\mathcal{C}}$ defined in Fig. 1 (we can also calculate the OTOC function for $W = c$, $V = c^\dagger$ [52]). Let us emphasize that the result (11) is valid not only in equilibrium but also out of equilibrium. For details of the numerical implementation, we refer to Ref. [34].

The results for the OTOC function $C(t) = -\langle[n^c(t),n^c(0)]^2\rangle$ are shown in Fig. 2 (red curves) for several U and β. As a comparison, we also plot the dynamical charge susceptibility $\chi(t) \equiv \chi(t,0)$ [Eq. (8)] (blue), which is a usual response function obeying causality. Both $C(t)$ and $\chi(t)$ grow after $t = 0$, peak out within $t \lesssim 1$, and gradually decay to zero. By definition, $C(t) \geqslant 0$, while $\chi(t)$ oscillates around zero. Initially the correlations build up as $C(t) \propto t^2$ and $\chi(t) \propto t$. Both of them show a long-time asymptotic behavior $\sim t^{-3}$, reflecting the power-law decay of the Green's function, $R^R_\alpha(t,0) \sim t^{-3/2}$ [52].

In the SYK model or other systems that show the anti–de Sitter (AdS)–conformal field theory (CFT) correspondence, one finds a separation of the relevant time scales; the time scale of the change of $C(t)$ (scrambling time) is longer than that of ordinary response functions such as $\chi(t)$ (thermalization time) by a factor of $\log N$ [9], where N is the number of sites for the SYK model or the number of colors in CFTs. In contrast, there is no clear separation of the two time scales in the FK model (Fig. 2), indicating that the AdS-CFT correspondence cannot be applied here. Given this circumstance, we do not clearly see an exponential growth (butterfly effect) of the deviation of the OTOC from the initial value. In this sense, the FK model does not describe a chaotic system, which is consistent with the expectation that systems with infinitely many conserved charges are not chaotic (and do not thermalize [39]).

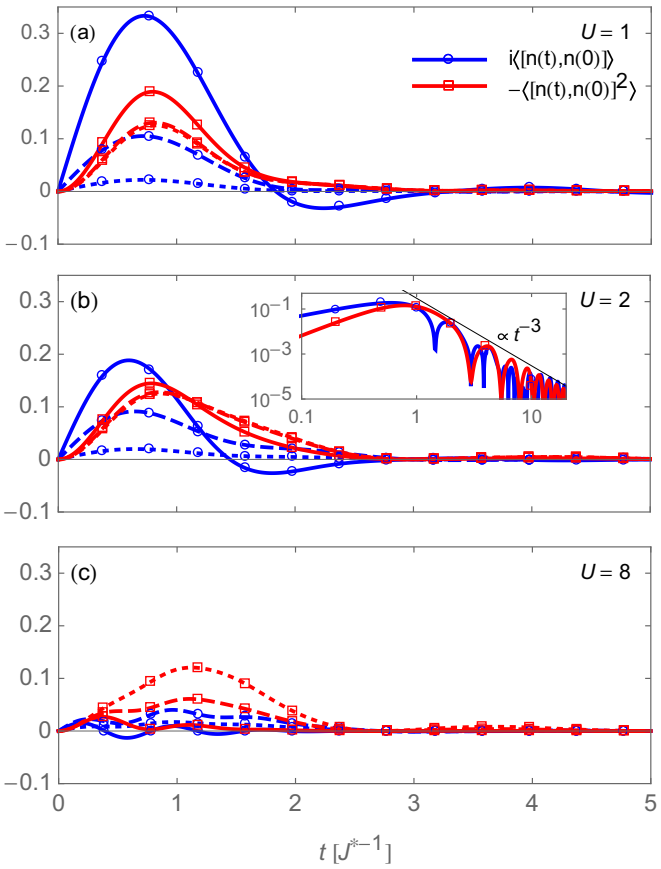

FIG. 2. Dynamical charge susceptibility $\chi(t)$ (blue curves) and out-of-time-ordered charge correlation function $C(t)$ (red) for the FK model with (a) $U = 1$, (b) $U = 2$, and (c) $U = 8$. The solid, dashed, and dotted curves correspond to $\beta = 10$, 0.5, and 0.1, respectively. The inset shows the corresponding log-log plot for the absolute values, compared with the asymptotic behavior $\propto t^{-3}$.

Nevertheless, if we look at the temperature dependence of $C(t)$ in Fig. 2, it is very different from that of the ordinary response function $\chi(t)$. As the temperature increases, the amplitude of $\chi(t)$ vanishes irrespective of U, whereas $C(t)$ is enhanced in the insulating phase [$U > 2$, Fig. 2(c)], more or less unchanged at the critical point [$U = 2$, Fig. 2(b)], and suppressed in the metallic phase [$U < 2$, Fig. 2(a)]. In particular, $C(t)$ remains nonvanishing and interaction dependent in the high-temperature limit, even though the dynamical charge correlations are completely suppressed ($\chi(t) \to 0$).

To quantify the temperature and interaction dependence of the OTOC at low energy, we compute the OTOC spectral function $C(\omega) = \int_0^\infty dt\, e^{i\omega t} C(t)$ and the dynamical charge susceptibility spectrum $\chi(\omega) = \int_0^\infty dt\, e^{i\omega t}\chi(t,0)$. $C(\omega = 0)$ measures how much the OTOC grows during the entire dynamics. Figure 3 plots $\chi(\omega = 0)$ and $C(\omega = 0)$ for several U and β. $\chi(\omega = 0)$ monotonically decreases as a function of U at arbitrary fixed temperature. At sufficiently low temperature, the charge gap opens in the insulating phase ($U > 2$), where $\chi(\omega = 0)$ vanishes. As the temperature increases, thermal excitations take place above the charge gap, leading to an increase in $\chi(\omega = 0)$ in the insulating phase. If the temperature further increases, charge correlations disappear and $\chi(\omega)$

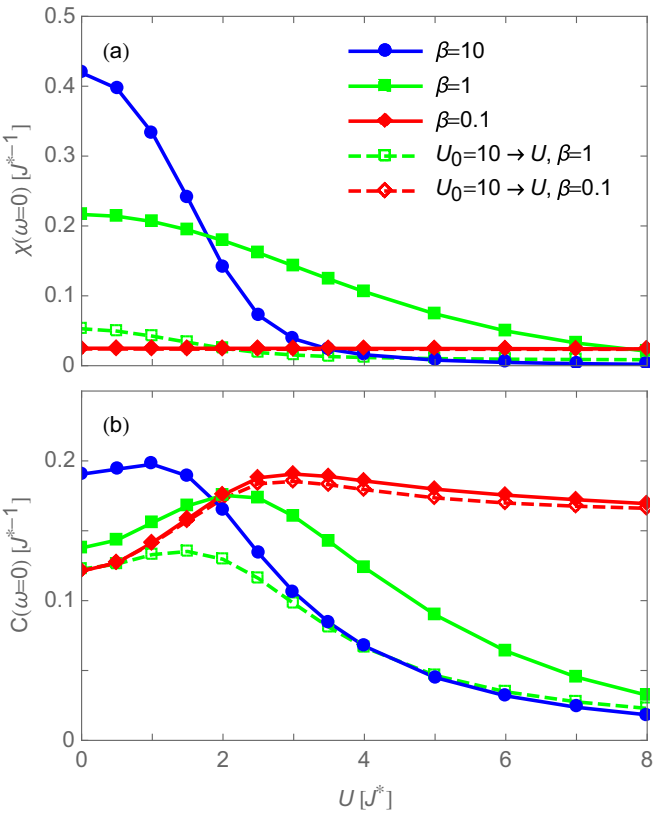

FIG. 3. Comparison between (a) the dynamical charge susceptibility $\chi(\omega)$ and (b) the OTOC spectral function $C(\omega)$ at $\omega = 0$ for the FK model. The dashed curves correspond to interaction quenches $U_0 = 10 \to U$ with initial temperatures $\beta = 1$ and 0.1.

approaches zero. In contrast, $C(\omega = 0)$ is a nonmonotonic function of U; it reaches the maximum at some intermediate coupling ($1 \lesssim U \lesssim 3$) around the metal-insulator transition point [Fig. 3(b)], and decays to zero in the $U \to \infty$ limit. In particular, the high-temperature limit of $C(\omega = 0)$, which is close to that of $\beta = 0.1$ in Fig. 3(b), shows a highly nontrivial nonzero spectral weight amplified in the insulating phase, whereas the ordinary response function becomes trivial. The overall temperature dependence of $C(\omega = 0)$ is similar to that of $C(t)$ discussed above.

Finally, let us discuss how to experimentally measure the OTOC $C(t)$ in many fermion systems. We consider ultracold atomic systems in an optical lattice. There have been several proposals on the measurement of OTOCs. One strategy is to take an interferometric approach with a qubit control [10–13]. Another approach is a time-reversal protocol [20,21]. Since ultracold atomic systems offer full control over the Hamiltonian parameters with negligible dissipation on the time scale of interest, we propose, based on the latter approach, a serial protocol (Fig. 4) implemented along the contour in Fig. 1(b) that is feasible with available experimental techniques for atomic gases.

We prepare a Mott-insulating state with the initial $U_0 = \infty$ tuned by a Feshbach resonance, and measure the number ($\equiv N_1$) of c particles at site j nondestructively. (Note that the Mott insulator is an eigenstate of the particle density.) Then we quench the interaction $U_0 = \infty \to U$ at $t = 0$, and let the

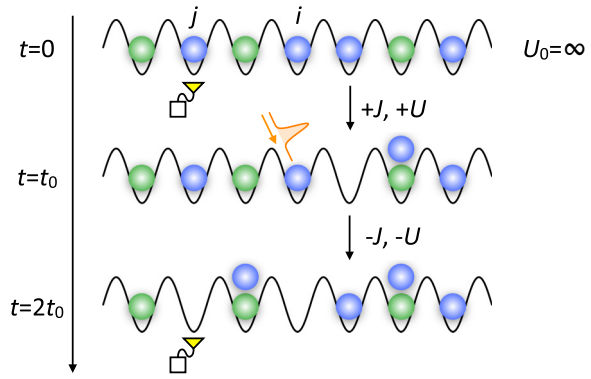

FIG. 4. Illustration of the proposed measurement protocol of the OTOC in ultracold atomic systems with two fermionic species (blue and green). At $t = t_0$, a local pulse is applied to site i, and at $t = 0$ and $t = 2t_0$ the particle density is measured at site j.

system time-evolve for a duration of t_0. At $t = t_0$, we apply an instantaneous local potential pulse $\delta H(t) = \varepsilon\delta(t - t_0)n_i^c(t)$ by using a focused laser to shift the energy level of site i [56]. After that, we change the hopping $J_{ij} \to -J_{ij}$ by shaking the lattice periodically [41], or applying a π pulse [57], or using a Raman process [58] to induce a π-phase shift in the kinetic term [59]. At the same time, we quench the interaction $U \to -U$. With these, we can flip the sign of the Hamiltonian, $H \to -H$ [60], which enables the system to effectively propagate backward in time (similar to a Loschmidt-echo experiment). After letting the system evolve for another t_0, we measure the c-particle density ($\equiv N_2$) at site j. We repeat this procedure to measure the expectation value of $2N_1N_2 - N_2$ [61]. If we expand it with respect to ε, we obtain

$$\begin{aligned}&\langle 2N_1N_2 - N_2\rangle \\ &= \mathrm{Tr}\big[\rho(0)\mathcal{U}(-t_0)e^{i\varepsilon n_i^c}\mathcal{U}(t_0)n_j^c\mathcal{U}(-t_0)e^{-i\varepsilon n_i^c}\mathcal{U}(t_0)\big(2n_j^c - 1\big)\big] \\ &= \big\langle n_j^c(0)\big\rangle + \varepsilon^2\big\langle\big[n_i^c(t_0),n_j^c(0)\big]^2\big\rangle + O(\varepsilon^3), \end{aligned} \tag{12}$$

where $\rho(0)$ is the initial density matrix, and $\mathcal{U}(t,t') \equiv \mathcal{U}(t - t')$. The leading-order contribution is exactly the OTOC $C(t)$ for the nonequilibrium system subject to the interaction quench $U_0 \to U$. In Fig. 3 (dashed curves), we show $\chi(\omega = 0)$ and $C(\omega = 0)$ for the interaction quench where the initial interaction is chosen to be large but finite ($U_0 = 10$). We can see the nonmonotonic behavior and characteristic temperature dependence of $C(\omega = 0)$, similar to the results obtained in equilibrium. This scheme is applicable not only to the FK model but also to the Hubbard model. To realize the FK model in ultracold atomic systems, we need a mass imbalance between two fermionic species.

To summarize, we have obtained an exact solution for the OTOCs of the FK model in the thermodynamic limit by generalizing the nonequilibrium DMFT to the extended Kadanoff-Baym contour $\tilde{\mathcal{C}}$. We find that the OTOC $C(t)$ is most enhanced around the metal-insulator transition point, and remains nontrivial in the high-temperature limit, which can be measured in ultracold atomic systems. Our work is a first step toward an analysis of OTOCs in more complicated fermionic lattice models, such as the Hubbard model. It is of interest to investigate whether those models, especially in the

"strange-metal" phase, show a chaotic behavior, and, if so, how fast they are scrambled.

We thank I. Danshita, T. Fukuhara, and I. Nakamura for stimulating discussions. N.T. is supported by JSPS KAKENHI Grant No. JP16K17729. P.W. acknowledges support from ERC Starting Grant No. 278023. M.U. acknowledges support by KAKENHI Grant No. JP26287088 and KAKENHI Grant No. JP15H05855.

[1] P. Hayden and J. Preskill, J. High Energy Phys. 09 (2007) 120.
[2] Y. Sekino and L. Susskind, J. High Energy Phys. 10 (2008) 065.
[3] S. H. Shenker and D. Stanford, J. High Energy Phys. 03 (2014) 067.
[4] S. H. Shenker and D. Stanford, J. High Energy Phys. 12 (2014) 046.
[5] A. Kitaev, talk given at Fundamental Physics Prize Symposium Nov. 10, 2014, https://www.youtube.com/watch?v=OQ9qN8j7EZI.
[6] A. Kitaev, talks at KITP (2015): http://online.kitp.ucsb.edu/online/entangled15/kitaev/, http://online.kitp.ucsb.edu/online/entangled15/kitaev2/ (unpublished).
[7] S. H. Shenker and D. Stanford, J. High Energy Phys. 05 (2015) 132.
[8] P. Hosur, X.-L. Qi, D. A. Roberts, and B. Yoshida, J. High Energy Phys. 02 (2016) 004.
[9] J. Maldacena, S. H. Shenker, and D. Stanford, J. High Energy Phys. 08 (2016) 106.
[10] B. Swingle, G. Bentsen, M. Schleier-Smith, and P. Hayden, Phys. Rev. A **94**, 040302 (2016).
[11] I. Danshita, M. Hanada, and M. Tezuka, arXiv:1606.02454.
[12] G. Zhu, M. Hafezi, and T. Grover, arXiv:1607.00079.
[13] N. Y. Yao, F. Grusdt, B. Swingle, M. D. Lukin, D. M. Stamper-Kurn, J. E. Moore, and E. Demler, arXiv:1607.01801.
[14] Y. Huang, Y.-L. Zhang, and X. Chen, Ann. Phys. (2016), doi:10.1002/andp.201600318.
[15] R. Fan, P. Zhang, H. Shen, and H. Zhai, arXiv:1608.01914.
[16] H. Shen, P. Zhang, R. Fan, and H. Zhai, arXiv:1608.02438.
[17] Y. Chen, arXiv:1608.02765.
[18] B. Swingle and D. Chowdhury, arXiv:1608.03280.
[19] R.-Q. He and Z.-Y. Lu, arXiv:1608.03586.
[20] M. Gärttner, J. G. Bohnet, A. Safavi-Naini, M. L. Wall, J. J. Bollinger, and A. M. Rey, arXiv:1608.08938.
[21] J. Li, R. Fan, H. Wang, B. Ye, B. Zeng, H. Zhai, X. Peng, and J. Du, arXiv:1609.01246.
[22] I. L. Aleiner, L. Faoro, and L. B. Ioffe, Annal. Phys. **375**, 378 (2016).
[23] A. I. Larkin and Y. N. Ovchinnikov, Sov. Phys. JETP **28**, 1200 (1969).
[24] S. Sachdev and J. Ye, Phys. Rev. Lett. **70**, 3339 (1993).
[25] S. Sachdev, Phys. Rev. X **5**, 041025 (2015).
[26] K. Jensen, Phys. Rev. Lett. **117**, 111601 (2016).
[27] J. Polchinski and V. Rosenhaus, J. High Energy Phys. 04 (2016) 001.
[28] J. Maldacena and D. Stanford, Phys. Rev. D **94**, 106002 (2016).
[29] J. Schwinger, J. Math. Phys. **2**, 407 (1961).
[30] L. V. Keldysh, Sov. Phys. JETP **20**, 1018 (1965).
[31] L. P. Kadanoff and G. Baym, *Quantum Statistical Mechanics* (Benjamin, New York, 1962).
[32] P. N. Butcher and D. Cotter, *The Elements of Nonlinear Optics* (Cambridge University Press, Cambridge, UK, 1998).
[33] J. K. Freericks, V. M. Turkowski, and V. Zlatić, Phys. Rev. Lett. **97**, 266408 (2006).
[34] H. Aoki, N. Tsuji, M. Eckstein, M. Kollar, T. Oka, and P. Werner, Rev. Mod. Phys. **86**, 779 (2014).
[35] L. M. Falicov and J. C. Kimball, Phys. Rev. Lett. **22**, 997 (1969).
[36] J. K. Freericks and V. Zlatić, Rev. Mod. Phys. **75**, 1333 (2003).
[37] A. E. Antipov, Y. Javanmard, P. Ribeiro, and S. Kirchner, Phys. Rev. Lett. **117**, 146601 (2016).
[38] J. K. Freericks, Phys. Rev. B **77**, 075109 (2008).
[39] M. Eckstein and M. Kollar, Phys. Rev. Lett. **100**, 120404 (2008).
[40] N. Tsuji, T. Oka, and H. Aoki, Phys. Rev. B **78**, 235124 (2008).
[41] N. Tsuji, T. Oka, and H. Aoki, Phys. Rev. Lett. **103**, 047403 (2009).
[42] E. Canovi, P. Werner, and M. Eckstein, Phys. Rev. Lett. **113**, 265702 (2014).
[43] A. J. Herrmann, N. Tsuji, M. Eckstein, and P. Werner, Phys. Rev. B **94**, 245114 (2016).
[44] A similar setup has been used in Refs. [9,22].
[45] W. Metzner and D. Vollhardt, Phys. Rev. Lett. **62**, 324 (1989).
[46] U. Brandt and C. Mielsch, Z. Phys. B **75**, 365 (1989).
[47] U. Brandt and C. Mielsch, Z. Phys. B **79**, 295 (1990).
[48] U. Brandt and C. Mielsch, Z. Phys. B **82**, 37 (1991).
[49] A. Georges, G. Kotliar, W. Krauth, and M. J. Rozenberg, Rev. Mod. Phys. **68**, 13 (1996).
[50] The generalized contour delta function on $\tilde{\mathcal{C}}$ is defined by $\int_{\tilde{\mathcal{C}}} d\bar{t}\, \delta_{\tilde{\mathcal{C}}}(t,\bar{t}) g(\bar{t}) = g(t)$ for an arbitrary contour function $g(t)$.
[51] One can also derive the same result by introducing an external field that couples to the c particle density and taking a functional derivative of the density with respect to the field.
[52] See Supplemental Material at http://link.aps.org/supplemental/10.1103/PhysRevA.95.011601 for the relation between the local and lattice susceptibilities, the long-time behavior of the OTOCs, and the fermionic OTOC for the FK model.
[53] A. M. Shvaika, Physica C **341-348**, 177 (2000).
[54] A. M. Shvaika, J. Phys. Stud. **5** (3/4), 349 (2001).
[55] J. K. Freericks and P. Miller, Phys. Rev. B **62**, 10022 (2000).
[56] In reality, the local pulse will not be perfectly delta-function-like. If one uses a pulse shape $f(t,\boldsymbol{r})$ with finite widths in time and space, we obtain the sum of contributions $\int dt' \int d\boldsymbol{r}' f(t-t',\boldsymbol{r}_i-\boldsymbol{r}')\langle[n^c_{\boldsymbol{r}'}(t'),n^c_j(0)]^2\rangle$.
[57] N. Tsuji, T. Oka, H. Aoki, and P. Werner, Phys. Rev. B **85**, 155124 (2012).
[58] D. Jaksch and P. Zoller, Ann. Phys. **315**, 52 (2005).
[59] During the sign reversal of the hopping, heating might occur. In this respect, the π-pulse method is superior to others since the system is driven only in a short time interval.
[60] If one uses a periodic drive, one has to quench $U \to -|J_0(A)|U$ [$J_0(A)$ is the zeroth-order Bessel function and A is the amplitude of the drive] so that the ratio between the hopping and interaction remains unchanged. In this case, the time after $t = t_0$ should be rescaled accordingly.
[61] Since $N_1, N_2 = 0,1$ for fermionic systems, it is enough to measure the parity of the particle density.